PRAMANA
— journal of
physics

Vol. 66, No. 4
April 2006
pp. 753–764

Hadron production near threshold

B K JAIN[1], N G KELKAR[2] and K P KHEMCHANDANI[1]
[1]Department of Physics, Tilak Bhavan, Vidyanagari, Santacruz (E), Mumbai 400 098, India
[2]Departamento de Fisica, Universidad de los Andes, Columbia
E-mail: brajesh_jain@vsnl.com

Abstract. Final state interaction effects in $pp \to p\Lambda K^+$ and $pd \to {}^3\mathrm{He}\ \eta$ reactions are explored near threshold to study the sensitivity of the cross-sections to the $p\Lambda$ potential and the ηN scattering matrix. The final state scattering wave functions between Λ and p and η and ^{3}He are described rigorously. The Λ production is described by the exchange of one pion and a K-meson between two protons in the incident channel. The η production is described by a two-step model, where in the first step a pion is produced. This pion then produces an η by interacting with another nucleon.

Keywords. Final state interaction; η-nucleus interaction; hyperon nucleon interaction; kaon production.

PACS Nos 13.75.-n; 25.40.Ve; 25.40.-h; 24.10.Eq

1. Introduction

Final state interaction is known to be a useful tool to study the interaction potential of unstable hadrons. Around threshold it becomes even more useful because at low energies the interactions manifest more richly due to coherent effects. With this motivation several high precision experiments have been done (and planned) on the production of hyperons and η-meson near threshold. They include the Λ and Σ production in pp collisions and η-meson production in pp and pd collisions. The objective of the hyperon production reaction had been to study the $\Lambda(\Sigma)N$ potential, while the η-meson reaction is aimed at exploring the possibility of the existence of the η-mesic nuclei besides determining the η-N interaction.

In this paper we present a rigorous (as far as possible) description of the $pp \to p\Lambda K^+$ and $pd \to {}^3\mathrm{He}\ \eta$ reactions. We compare our calculated cross-sections for both the reactions with the available experimental data. We study the sensitivity of the calculated cross-sections to the ΛN potential and the ηN interaction (for details see refs [1,2]).

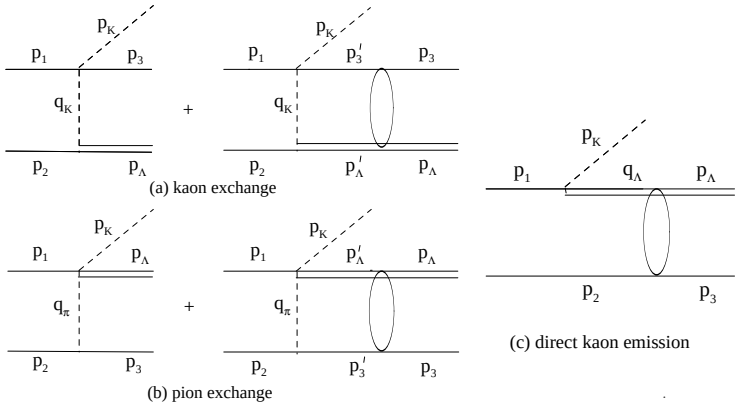

Figure 1. Diagrams for the $pp \to K^+\Lambda p$ reaction: (**a**) kaon exchange, (**b**) pion exchange, (**c**) direct kaon emission. The ellipses indicate the final state interactions of the Λ and proton.

2. $pp \to p\Lambda K^+$ reaction

Exclusive data on total cross-section exist from COSY on $pp \to K^+\Lambda p$ and $pp \to K^+\Sigma p$ reactions up to an excess energy of 60 MeV. On the missing mass spectra, however, only the inclusive data exist. Below Σ threshold these data predominantly correspond to the $pp \to K^+\Lambda p$ reaction. The main objective of our calculations is to study the effect of the final state interaction between the proton and Λ in the $pp \to K^+\Lambda p$ reaction and make an intercomparison of the calculated cross-sections using different available models of the hyperon-nucleon (YN) interaction. The differences in the various models of the YN interaction are expected to show up in the Λp invariant mass spectra because they involve Λp at different relative momenta starting from zero at threshold. These spectra should therefore be sensitive to the differences in the contributions of the various partial waves in different potentials for the Λp scattering and to the opening of the Σ production channel where the ${}^3S_1$–${}^3D_1$ coupled channels are important. We use the missing mass data for our studies in this paper.

As for the reaction mechanism, guided by the earlier investigations, we assume that it proceeds by the exchange of a pion or a kaon between the two protons in the entrance channel and neglect any contributions from heavier mesons like ρ and K^*. In the case of π exchange, one of the interacting protons can be excited by the exchanged pion to any of the relevant N^* resonances, which then decays to a K^+ and Λ. In the case of kaon exchange, the K^+ and Λ are produced directly. In addition to these meson exchange diagrams, we also include the DKE diagram, where the proton in the initial state dissociates into K^+ and an off-shell Λ, which by its interaction with the second proton is brought on-shell. However, its contribution is expected to be small because the intermediate Λ is *far* off-shell.

In our work we have included all the production diagrams shown in figure 1. Since it is not possible to fix the relative sign between the amplitudes corresponding to the pion and kaon exchange diagrams we choose to retain an additive sign between these

amplitudes. The diagrams arising due to antisymmetrization of the two protons in the initial state have also been included. The amplitudes for $\pi^0 p \to K^+\Lambda$ and $K^+p \to K^+p$ at the kaon production vertices are constructed from the existing experimental data. Since these amplitudes fit the experimental data, they implicitly include the excitation of the resonances in πp scattering. The off-shell extrapolation is incorporated through a form factor.

In the final state we have three particles, K^+, Λ and p. Since the interaction of K^+ with other two hadrons is weak, we consider only the interaction between p and Λ. For the hyperon–nucleon potential, V_{YN}, currently there exists meson exchange models which are similar in construction to the models of the well-known nucleon–nucleon (NN) interaction. The prominent ones among these are the Nijmegen and Jülich potentials [3,4]. The free model parameters of the YN interaction in these models are fixed using the cross-section data on YN scattering.

The final state Λp wave function $\Psi^{-*}_{\Lambda p}$ consists of a plane wave and a scattered wave and can be written as

$$\Psi^{-*}_{\Lambda p} = \langle \vec{p}_\Lambda\, \vec{p}_3| + \Psi^*_{\rm scat}, \tag{1}$$

where $\Psi^*_{\rm scat}$ is given in terms of the t-matrix for Λp scattering as,

$$\Psi^*_{\rm scat} = \langle \vec{p}_\Lambda\, \vec{p}_3|\, t_{\Lambda p\to\Lambda p} G_0. \tag{2}$$

Here G_0 is the plane wave propagator for the Λp system in the intermediate state. Since the Λp momentum in this state is not fixed, the matrix $t_{\Lambda p\to\Lambda p}$ in the above expression is necessarily off-shell. The phase shift approximation to $\Psi_{\rm scat}$ is obtained by taking this t-matrix on-shell. In r-space this implies approximating the scattered wave function by its asymptotic form.

To obtain $\Psi_{\rm scat}$, we consider the ΛN as well as the ΣN channels together. $\Psi_{\rm scat}$ is thus obtained by solving

$$t_{\Lambda p\to\Lambda p} \;=\; V_{\Lambda p\to\Lambda p} + \langle \Lambda p|VGt|\Lambda p\rangle, \tag{3}$$

where V, G and t are (2×2) matrices. G is the free Λp or ΣN propagator between two scatterings. The diagonal matrix elements describe respectively the $\Lambda p \to \Lambda p$ and $\Sigma N \to \Sigma N$ channels while the off-diagonal elements give the $\Lambda p \to \Sigma N$ and $\Sigma N \to \Lambda p$ transitions. Thus the constructed $t_{\Lambda p}$ includes the effect of the ΣN channel in Λp scattering. We construct $t_{\Lambda p}$ using the Nijmegen soft-core [3] and Jülich [4] YN potentials.

All our calculations are done using the partial wave expansion at every stage. Thus from the calculation point of view, our results are exact and carry all the details of the final state interaction and the Λ-production amplitude $V^x_{pp\to K^+\Lambda p}$.

2.1 *Results and discussion*

In figure 2 we show the differential cross-section $\mathrm{d}^2\sigma/\mathrm{d}\Omega_K \mathrm{d}W$ as a function of the invariant mass W of the Λp pair. Ω_K is the solid angle of the emitted kaon in the laboratory system. The proton beam energy is 2.3 GeV and the kaon angle is fixed at 10°.

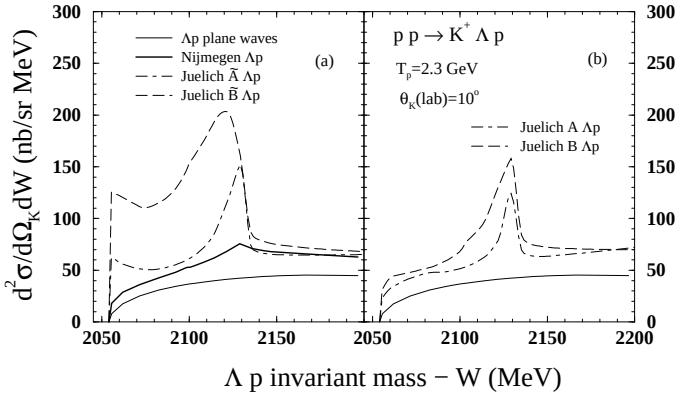

Figure 2. Λp invariant mass spectra at 2.3 GeV beam energy for the exclusive $pp \to K^+\Lambda p$ reaction calculated using different potentials for the Λp final state interaction. (**a**) Thick solid line uses the Nijmegen soft-core potential, dash–dotted and dashed curves are calculations using versions $\tilde{A}$ and $\tilde{B}$ respectively of the energy independent Jülich potential. (**b**) Calculations using energy dependent versions A (dash–dotted curve) and B (dashed curve) of the Jülich potential. The thin solid lines in (a) and (b) are the results using plane waves for the Λ and proton in the final state.

The thick solid line in figure 2a is our full calculation for the $pp \to K^+\Lambda p$ reaction with the Nijmegen potential for the Λp interaction. The dash–dotted and dashed lines are respectively the full calculations with the energy independent versions $\tilde{A}$ and $\tilde{B}$ of the Jülich potentials. The thin solid line is the calculation using plane waves for the Λ and proton. In figure 2b we show the calculations using the energy-dependent versions A and B of the Jülich potentials. We observe that all the curves with the Λp interaction included show an enhancement of the cross-sections over the plane wave results, along the entire mass spectrum. The extent of the enhancement and the detailed structure in the spectrum, however, depend upon the choice of V_{YN}. As we see in figure 2a, the Jülich potential $\tilde{A}$ produces a prominent cusp at the Σ threshold which is less prominent in the case of the Nijmegen potential. A rounded peak in the cross-section at the Σ threshold is produced by the Jülich potential $\tilde{B}$. This peak is shifted in position as compared to the cusps. Similarly, at the Λ threshold we see sharp peaks or bumps in figures 2a and 2b, depending on the type of potential used.

All the above-mentioned potentials though have been constructed by fitting to the same set of ΛN elastic scattering data, they differ in their weightage of the different partial waves.

In figure 3 we compare our calculated cross-sections with the inclusive data of ref. [5] on the $pp \to K^+YN$ reaction. As mentioned above, below the threshold for the Σ production ($W = 2128$ MeV) the data correspond entirely to that for the $pp \to K^+\Lambda p$ reaction. The steep rise in the measured cross-sections at the Σ threshold is due to the opening of the Σ producing channels $pp \to K^+\Sigma^0 p$ and $pp \to K^+\Sigma^+ n$.

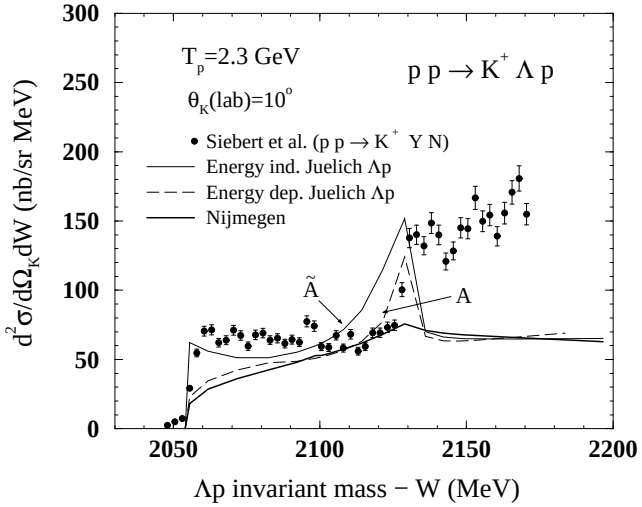

Figure 3. Comparison of calculated invariant Λp mass spectra for the $pp \to K^+\Lambda p$ reaction with the available inclusive data on the $pp \to K^+YN$ reaction. The data are from ref. [5]. The thick solid line is the calculation using the Nijmegen soft-core Λp potential. The thin solid line and dashed line are respectively the results using energy independent and dependent versions of the Jülich potential A.

We see that, while both the Nijmegen and Jülich potentials give the general trend of the data below the Σ threshold, in details they compare differently. The cross-sections calculated using Jülich $\tilde{A}$ agree somewhat with data at the Λ threshold. The peak at the Σ threshold is more pronounced with the Jülich potentials than with the Nijmegen potential. To constrain the YN potentials further, we need exclusive data on the Λp and ΣN channels.

Next we investigate the accuracy of the on-shell approximation to the Λp final state interaction, which very often is used in the FSI calculations. For this we use the Nijmegen YN potential.

In figure 4, the thick solid line is our calculation with the off-shell Λp t-matrix as in figure 2. The thin solid line is obtained by replacing the off-shell matrix elements $\langle p_{\Lambda p}|t^{\Lambda p\to\Lambda p}|q\rangle$ in our calculations by the on-shell ones $\langle p_{\Lambda p}|t^{\Lambda p\to\Lambda p}|p_{\Lambda p}\rangle$. The scale for this curve is indicated on the right-hand side of the figure. The scale for all other curves is indicated on the left. We see that the on-shell approximation results are much larger in magnitude and different in shape compared to those due to the correct t-matrix. This difference, however, is reduced to a great extent by multiplying the on-shell t-matrix by an off-shell form factor. The results for a form factor $F_{\Lambda p} = (p_{\Lambda p}^2 + \beta^2)/(q^2 + \beta^2)$ with $\beta = 1.36$ fm^{-1} are shown by the dashed curve of figure 4. The form factor causes a large reduction of the cross-sections and the pronounced peak at the Λ threshold flattens out. Still a considerable difference between this prescription and the correct calculation persists. This difference can now be reduced and the calculated 'on-shell' results can be brought nearer to the experimental measurement, by arbitrarily adjusting the parameters in the reaction

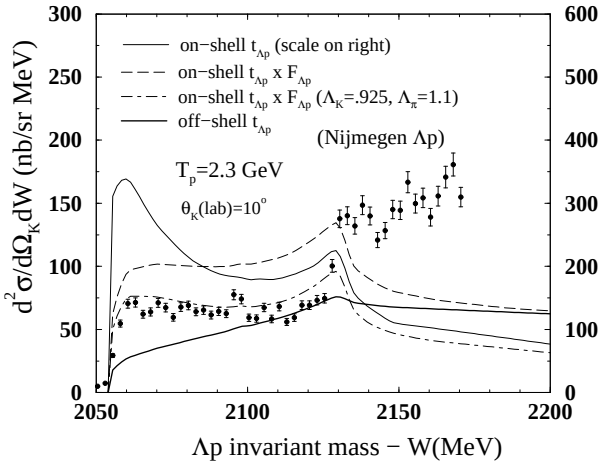

Figure 4. Effects of on-shell approximations of the final state Λp interaction on the Λp mass spectra for the $pp \to K^+\Lambda p$ reaction. Calculations are done using the Nijmegen Λp potential. The thin solid line is the calculation (with scale given on the right) using on-shell matrix elements of the t-matrix for $\Lambda p \to \Lambda p$. Dashed curve is obtained by multiplying the on-shell matrix elements of $t^{\Lambda p \to \Lambda p}$ by a form factor $F_{\Lambda p}$ (scale on left). Dash–dotted curve is obtained by reducing the values of Λ_K and Λ_π in a calculation similar to that of the dashed curve. The thick solid line uses the off-shell matrix elements of $t^{\Lambda p \to \Lambda p}$ (as used throughout this work). The solid curves and the dashed curve show results using $\Lambda_K = 1.2$ and $\Lambda_\pi = 1.3$ GeV. The data are the same as in figure 3.

vertices for the $pp \to K^+\Lambda p$ transition. The dash–dotted curve in figure 4 which agrees with data is the result for Λ_π, Λ_K and $g_{KN\Lambda}$ equal to 1.1 GeV, 0.925 GeV and -13.26 respectively at the reaction vertex. However, this way of constraining the transition amplitude parameters is obviously misleading.

2.2 *Summary*

In summary we conclude the following:

1. The cross-sections with FSI included are found to be enhanced compared to the plane-wave results for both the Nijmegen and Jülich potentials. However, the magnitude of the cross-sections and the structure in them differ a lot for the two potentials. The general trend of the experimental data is produced by these calculations but in details they compare differently with data. Thus the exclusive data on the $pp \to K^+\Lambda p$ reaction can be very useful to differentiate amongst different V_{YN}.
2. We have made a comparison of our results with the off-shell t-matrix for $\Lambda p \to \Lambda p$ scattering with those using the on-shell t-matrix. The on-shell results (even after multiplying by the off-shell form factor) overestimate the results

obtained using the off-shell Λp t-matrix. Therefore, attempts to represent the FSI between the Λ and proton by phase shifts (with an off-shell form factor) may not represent the FSI accurately. This can lead to errors in conclusions about the parameters associated with the $pp \to K^+\Lambda p$ transition interaction, if the same are adjusted to fit the data in this approach.

3. $pd \to {}^3\mathrm{He}\,\eta$ reaction

Experimental data on the $pd \to {}^3\mathrm{He}\,\eta$ reaction exist close to threshold. Compared to the π^0 production they reveal some surprising features [6,7]. In spite of the large momentum transfer involved in η production compared to that in pion production, the cross-section for $pd \to {}^3\mathrm{He}\,\eta$ is large and comparable with that for $pd \to {}^3\mathrm{He}\,\pi^0$. The energy dependence of the two reactions near threshold is also very different. The $pd \to {}^3\mathrm{He}\,\eta$ reaction shows a much rapid variation, with the threshold amplitude falling by a factor of 3.75 over an η centre of mass energy of 11 MeV. We present a rigorous calculation for these cross-sections, which also reproduce the experimental findings (for details see ref. [2]).

Due to the large mass of the η meson, the momentum transfer involved in this reaction is large. It is 900 MeV/c at threshold and reduces to 500 MeV/c by about 1 GeV above threshold. As a result of this the three-body mechanism which allows the momentum transfer to be shared amongst three nucleons dominates. We assume that the three nucleons share the large momentum transfer through a two-step process where the incident proton interacts with a nucleon in the deuteron to produce a pion which then interacts with the other nucleon in the deuteron to produce an η meson. The $p\,d \to {}^3\mathrm{He}\,\eta$ reaction, thus, proceeds via the $NN \to \pi d$ and $\pi N \to \eta N$ reactions.

3.1 η-^{3}*He elastic scattering T-matrix*

In the present work we study the $pd \to {}^3\mathrm{He}\,\eta$ reaction near threshold using the three-body mechanism mentioned above. We express the $\eta\,{}^3\mathrm{He}$ relative wave function in terms of the Lippmann–Schwinger equation involving the T-matrix for $\eta\,{}^3\mathrm{He}$ elastic scattering. This T-matrix is evaluated using a method of few-body equations called 'finite rank approximation' [8], where the scattering of η-meson from each nucleon is written after considering its earlier scattering from other two nucleons. Such a T-matrix thus goes much beyond the impulse approximation T-matrix. The nucleus in this approximation is, however, assumed to remain in its ground state in the intermediate state.

Within this approximation, the $\eta\,{}^3\mathrm{He}$ T-matrix is given as

$$T(\vec{k}',\,\vec{k}\,;z) = \langle\vec{k}';\psi_0|T^0(z)|\vec{k};\psi_0\rangle + \varepsilon\int \frac{\vec{D}''}{(2\pi)^3}\frac{\langle\vec{k}';\psi_0|T^0(z)|\vec{k}'';\psi_0\rangle}{(z-\frac{k''^2}{2\mu})(z-\varepsilon-\frac{k''^2}{2\mu})}T(\vec{k}'',\,\vec{k}\,;\,z), \tag{4}$$

where $z = E - |\varepsilon| + i0$. E is the energy associated with η-nucleus relative motion and μ is the reduced mass of the η-nucleus system. The operator T^0 describes the scattering of η-meson from nucleons fixed in their space position within the nucleus. The matrix elements for T^0 are given as

$$\langle \vec{k}'; \psi_0 | T^0(z) | \vec{k}; \psi_0 \rangle = \int \mathrm{d}\vec{r}\, |\psi_0(\vec{r})|^2 T^0(\vec{k}', \vec{k}; \vec{r}; z), \tag{5}$$

where

$$T^0\,(\vec{k}',\, \vec{k}\,; \vec{r}\,; z) = \sum_{i=1}^{A} T_i^0\,(\vec{k}',\, \vec{k}\,; \vec{r}_i\,; z) \tag{6}$$

T_i^0 is the t-matrix for the scattering of the η-meson from the ith nucleon in the nucleus, with the rescattering from the other (A-1) nucleons included. It is given as,

$$T_i^0\,(\vec{k}',\, \vec{k}\,; \vec{r}_i\,; z) = t_i(\vec{k}',\, \vec{k}\,; \vec{r}_i\,; z) + \int \frac{\mathrm{d}\vec{k}''}{(2\pi)^3}\, \frac{t_i(\vec{k}',\, \vec{k}''\,; \vec{r}_i\,; z)}{z - \frac{k''^2}{2\mu}} \sum_{j \neq i} T_j^0(\vec{k}'',\, \vec{k}\,; \vec{r}_j\,; z). \tag{7}$$

The t-matrix for elementary η-nucleon scattering, t_i, is written in terms of the two-body ηN matrix $t_{\eta N}$ as

$$t_i(\vec{k}',\, \vec{k}\,; \vec{r}_i\,; z) = t_{\eta N}(\vec{k}',\, \vec{k}\,; z)\, \exp[\, i(\vec{k} - \vec{k}\,') \cdot \vec{r}_i]. \tag{8}$$

The ^{3}He wave function ψ_0, required in the calculation of $T_{\eta\,^3\mathrm{He}}$ is taken to be of the Gaussian form.

Since there exists a lot of uncertainty in the knowledge of the η-nucleon interaction, we use three different prescriptions of the η-N t-matrix, $t_{\eta N \to \eta N}$, leading to different values of the η-N scattering length. All these t-matrices are the result of the coupled channel calculations including the πN and ηN channels and dominated by the $S_{11}N^*$ resonance. It is important to note that the parameters in all the coupled channel t-matrices mentioned above are adjusted to reproduce the data on the $\pi N \to \eta N$ reaction, but the values of $a_{\eta N}$ deduced from them are different (see table 1).

3.2 *Production mechanism*

As mentioned earlier, we assume the η production in $pd \to {}^3\mathrm{He}\,\eta$ to proceed through a two-step process via the $NN \to \pi d$ and $\pi N \to \eta N$ reactions as shown in figure 5.

The amplitude for the $p\,d \to {}^3\mathrm{He}\,\eta$ reaction can be written within this model as

$$\begin{aligned}\langle |T_{pd \to {}^3\mathrm{He}\,\eta}| \rangle = i \int & \frac{\mathrm{d}\vec{p}_1}{(2\pi)^3} \frac{\mathrm{d}\vec{p}_2}{(2\pi)^3} \\ & \times \sum_{\mathrm{int}\, m's} \langle pn|d\rangle \langle \pi^+\, d|T_{pp \to \pi^+ d}|p\,p\rangle \\ & \times \frac{1}{(k_\pi^2 - m_\pi^2 + i\varepsilon)} \langle \eta\, p\,|\, T_{\pi N \to \eta p}|\pi^+\, n\rangle\ \langle\, {}^3\mathrm{He}|pd\rangle, \end{aligned} \tag{9}$$

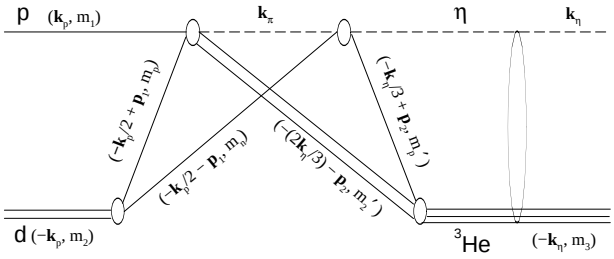

Figure 5. Diagram of η production in the $pd \rightarrow {}^3\mathrm{He}\,\eta$ reaction with a two-step process. The ellipse indicates the final state interaction of ^{3}He and η.

where the sum runs over the spin projections of the intermediate particles. The spin projections and momenta of the interacting particles are as shown in figure 5. k_π is the four momentum of the intermediate pion which could either be π^+ or π^0. In the case of an intermediate π^0, the matrix element for $pd \rightarrow {}^3\mathrm{He}\,\eta$ is half of that written above for π^+. Hence we calculate the T-matrix as in eq. (9) and multiply it by a factor of 3/2 to account for the intermediate π^0. Each of the individual matrix elements in the above equation is expressed in terms of partial wave expansions. The matrix elements for the $pp \rightarrow \pi^+ d$ reaction, parametrized in terms of the available experimental data, are taken from ref. [9]. For the $\pi^+ n \rightarrow \eta p$ reaction, we use the coupled channel t-matrix of ref. [10], mentioned in the previous section. The matrix elements $\langle pn|d\rangle$ and $\langle {}^3\mathrm{He}|pd\rangle$ consist of the deuteron and helium wave functions in momentum space. We use the deuteron wave function from ref. [11] where its analytical parametrization was done with a Paris potential. This wave function reproduces the known low-energy properties and the electromagnetic form factor of the deuteron well. For the ^{3}He wave function, we use the parametrization given in ref. [12]. The values of the parameters in [12] were obtained by fitting the wave function to the variational calculations of Schiavilla *et al* [13] using the Urbana force.

3.3 *Results and discussion*

The reaction $pd \rightarrow {}^3\mathrm{He}\,\eta$ has been studied at Saturne [6,7] for proton energies between 0.2 and 11 MeV above threshold. Taking out the phase-space factor, the spin averaged amplitude can be defined as

$$|f|^2 = \frac{k_p}{k_\eta} \cdot \frac{\mathrm{d}\sigma}{\mathrm{d}\Omega}_{cm}, \tag{10}$$

where k_p and k_η are the proton and η momenta in the centre of mass system. The data on $|f|^2$ (see figure 6) drops rapidly (by about a factor of 3.75) from threshold to 0.4 fm^{-1} momentum (corresponding to 11 MeV energy) above threshold.

In figure 6 we compare our calculations of $|f|^2$ (at $\theta_\eta = 180°$) with and without the inclusion of the $\eta\,{}^3$He final state interaction (FSI), with the data from refs [6,7].

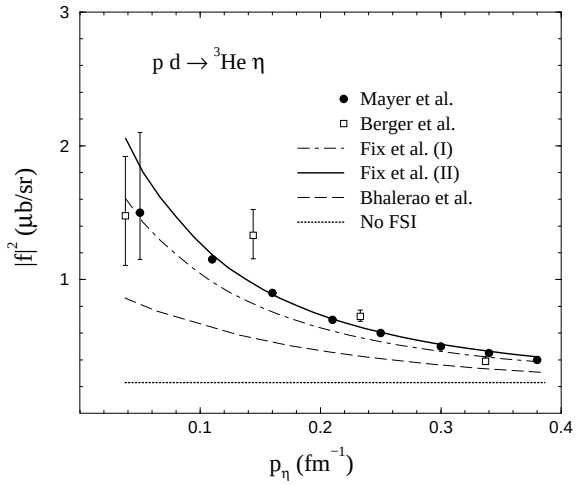

Figure 6. The square of the $pd \rightarrow {}^3\mathrm{He}\,\eta$ amplitude as a function of the η momentum in the centre of mass. The data are from refs [6,7]. The dotted line is the calculation of the present work without including the FSI. The solid, dash–dotted and dashed lines are the calculations including FSI with different prescriptions of elementary t-matrices.

The dotted line in figure 6 is our calculation without FSI and can be seen to be a constant as a function of energy. The dash–dotted, solid and dashed curves are the results obtained using the t-matrix of ref. [14], with parameter sets (I) and (II), and that of ref. [10] respectively. We see that the FSI is responsible for changing the shape of $|f|^2$ from a constant to a rapidly falling one as a function of energy.

In figure 7 we study the off-shell effects in the FSI. In our work we describe the $\eta\,{}^3$He final state interaction through an off-shell T-matrix for $\eta\,{}^3$He scattering. Since previous estimates of FSI in literature have been made using on-shell amplitudes, it is important to check the validity of such an approximation. The $\eta\,{}^3$He T-matrix appears in the integral in the Lippmann–Schwinger equation for the η-^{3}He elastic scattering wave function. This integral can be split into the principal value and pole term. Retaining only the pole term and setting the principal value (which involves the off-shell $\eta\,{}^3$He scattering) to zero, we get the dash–dotted line in figure 7. The solid line represents the full calculation. Both the curves use the prescription of ref. [14] with parameter set (II) for the elementary t-matrix. Thus we see that including the off-shell effects only produces the proper energy dependence of $|f|^2$ in addition to increasing its magnitude as compared to the pole term calculation.

Since there is much interest in the question whether the strong attractive ηN interaction retains its character in nuclear medium and gives rise to η mesic nuclei, we calculate the scattering length corresponding to our calculated η-^{3}He T-matrix. For the three elementary η-N scattering matrices used in our calculations, in table 1 we list these scattering lengths along with the corresponding elementary scattering lengths. These scattering lengths as we see, due to multiple scattering gets changed even in their signs for the Fix I and Fix II η-N matrices. For the weaker Bhalerao *et al* scattering matrix, however, the sign remains unchanged. This indicates that

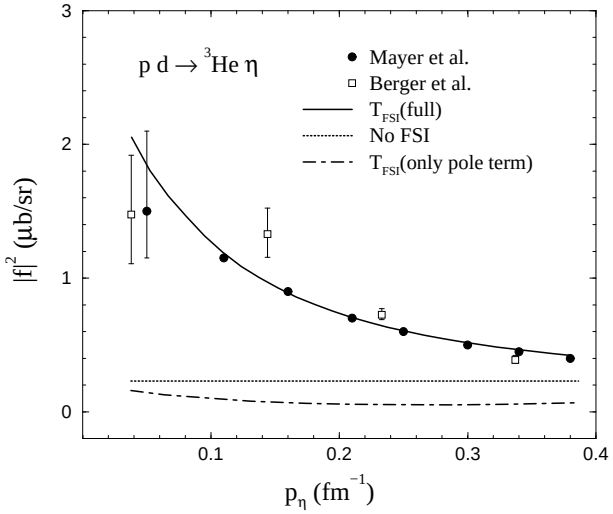

Figure 7. The solid and dotted lines and the data are as in figure 6. The dash–dotted line is the FSI calculation retaining only the pole term in the LS equation. We have used the elementary t-matrix $t_{\eta N \to \eta N}$ of ref. [14] with parameter set (II).

probably for strong η-N t-matrix the η-mesic nucleus might not exist for the ^{3}He nucleus. For not so attractive t-matrix, however, the probability for the existence of such a nucleus may be there.

3.4 *Summary*

The $pd \to {}^3\mathrm{He}\,\eta$ reaction has been studied in the present work within a two-step model, incorporating the final state interaction (FSI) of the ^{3}He nucleus and η-meson in a rigorous way. The peculiar behaviour of the cross-section for this η producing reaction as compared to a similar pion producing reaction $pd \to {}^3\mathrm{He}\,\pi^0$ is seen to originate due to the interaction between ^{3}He and η. The FSI changes the energy dependence of the squared amplitude from a constant (without FSI) to one which falls by a factor of about 4, from threshold to 11 MeV above threshold. We incorporate the FSI through an off-shell T-matrix for $\eta\,{}^3$He elastic scattering. This T-matrix is evaluated by numerically solving few-body equations which include the

Table 1. Scattering lengths (fm).

Reference	ηN	η-^{3}He
Fix I [14]	$0.75 + i0.27$	$-2.49 + i4.93$
Fix II [14]	$0.88 + i0.41$	$-2.35 + i5.67$
Bhalerao and Liu [10]	$0.28 + i0.19$	$+0.82 + i2.0$

nuclear binding effects. The off-shell effects in $\eta\,^3$He scattering are found to be important in the calculation of the $pd \to {}^3\mathrm{He}\,\eta$ reaction near threshold. Earlier investigations of this reaction involving on-shell and approximate ways of calculating the FSI should hence be treated with caution.

The η nucleus interaction has generated a lot of interest in the past few years, particularly due to the possibility of forming η mesic nuclei. Since it is difficult to obtain data on elementary η nucleon scattering, little is known about the ηN interaction. The scattering length in ηN scattering is a much debated quantity and different estimates and limiting values (for the possible formation of an η mesic nucleus) of this parameter exist in literature. Within the models used in the present work we find that values of the ηN scattering length, $\mathrm{Re}\,a_{\eta N} \sim 0.75$ to 0.9 and $\mathrm{Im}\,a_{\eta N} \sim 0.3$ to 0.4 lead to a good reproduction of the $pd \to {}^3\mathrm{He}\,\eta$ data near threshold.

Acknowledgements

This work was supported by a grant from the Department of Science and Technology, Government of India.

References

[1] N G Kelkar and B K Jain, *Int. J. Mod. Phys.* **E9**, 431 (2000)
[2] K P Khemchandani, N G Kelkar and B K Jain, *Nucl. Phys.* **A708**, 312 (2002)
[3] P M M Maessen, Th A Rijken and J J de Swart, *Phys. Rev.* **C40**, 2226 (1989)
[4] B Holzenkamp, K Holinde and J Speth, *Nucl. Phys.* **A500**, 485 (1989)
A Reuber, K Holinde and J Speth, *Nucl. Phys.* **A570**, 543 (1994)
[5] Siebert *et al*, *Nucl. Phys.* **A567**, 819 (1994)
[6] B Mayer *et al*, *Phys. Rev.* **C53**, 2068 (1996)
[7] J Berger *et al*, *Phys. Rev. Lett.* **61**, 919 (1988)
[8] V B Belyaev, Lectures on the theorem of few body systems in: *Springer series in nuclear and particle physics*, 1990
[9] R A Arndt, I Strakovsky, R L Workman and D A Bugg, *Phys. Rev.* **C48**, 1926 (1993); The amplitudes can be obtained from the SAID program available on internet (http://gwdac.phys.gwu.edu). To access via telnet, connect to 'gwdac.phys.gwu.edu' with login 'said' and no password
[10] R S Bhalerao and L C Liu, *Phys. Rev. Lett.* **54**, 865 (1985)
[11] M Lacombe, B Loiseau, R Vinh Mau, J Côté, P Pirés and R de Tourreil, *Phys. Lett.* **B101**, 139 (1981)
[12] J F Germond and C Wilkin, *J. Phys.* **G14**, 181 (1988)
[13] R Schiavilla, V R Pandharipande and R B Wiringa, *Nucl. Phys.* **A449**, 219 (1986)
[14] A Fix and H Arenhövel, *Nucl. Phys.* **A697**, 277 (2002)